Thermal Annealing Treatment to Achieve Switchable and Reversible Oleophobicity on Fabrics

Citation: Chhatre, Shreerang S. et al. "Thermal Annealing Treatment to Achieve Switchable and Reversible Oleophobicity on Fabrics." Langmuir 25.23 (2009): 13625-13632.

As Published: http://dx.doi.org/10.1021/la901997s

Publisher: American Chemical Society

Persistent URL: http://hdl.handle.net/1721.1/61628

Version: Author's final manuscript: final author's manuscript post peer review, without publisher's formatting or copy editing

Thermal annealing treatment to achieve switchable and reversible oleophobicity on fabrics

Shreerang S. Chhatre[1], *Anish Tuteja*[1], *Wonjae Choi*[2], *Amélie Revaux*[1], *Derek Smith*[1], *Joseph M. Mabry*[3], *Gareth H. McKinley*[2*] *and Robert E. Cohen*[1*]

[1] Shreerang S. Chhatre, Dr. Anish Tuteja, Amélie Revaux, Derek Smith and Prof. Robert E. Cohen

Department of Chemical Engineering, Massachusetts Institute of Technology, Cambridge, MA 02139 (USA)

[2] Dr. Wonjae Choi and Prof. Gareth H. McKinley

Department of Mechanical Engineering, Massachusetts Institute of Technology, Cambridge, MA 02139 (USA)

[3] Dr. Joseph M. Mabry

Space and Missile Propulsion Division, Air Force Research Laboratory, Edwards Air Force Base, CA 93524 (USA)

***: Corresponding authors**

Prof. Robert E. Cohen (recohen@mit.edu)

Prof. Gareth H. McKinley (gareth@mit.edu)

RECEIVED DATE

ABSTRACT

Surfaces which are strongly non-wetting to oil and other low surface tension liquids can be realized by trapping microscopic pockets of air within the asperities of a re-entrant texture and generating a solid-liquid-vapor composite interface. For low surface tension liquids like hexadecane (γ_{lv} = 27.5 mN/m), this composite interface is metastable due to the low value of the equilibrium contact angle. Consequently pressure perturbations can result in an irreversible transition of the metastable composite interface to the fully-wetted interface. In this work, we use a simple dip-coating and thermal annealing procedure to tune the liquid wettability of commercially available polyester fabrics. A mixture of 10 % 1H,1H,2H,2H-heptadecafluorodecyl polyhedral oligomeric silsesquioxane (fluorodecyl POSS) and 90 % polyethyl methacrylate (PEMA) is used to uniformly coat the fabric surface topography. Contact angle measurements show that a robust metastable composite interface with high apparent contact angles can be supported for hexadecane (γ_{lv} = 27.5 mN/m) and dodecane (γ_{lv} = 25.3 mN/m). To tune the solid surface energy of the coated surface, we also developed a reversible treatment using thermal annealing of the surface in contact with either dry air or water. The tunability of the solid surface energy along with the inherent re-entrant texture of the polyester fabric result in reversibly switchable oleophobicity between a highly non-wetting state and a fully wetted state for low surface tension liquids like hexadecane and dodecane. This tunability can be explained within a design parameter framework which provides a quantitative criterion for the transition between the two states, as well as accurate predictions of the measured values of the apparent contact angle (θ^*) for the dip-coated polyester fabrics.

KEYWORDS – Dip-coating, oleophobicity, switchable wettability, surface reconstruction

Introduction

When a liquid in contact with a flat surface attains thermodynamic equilibrium, it exhibits a contact angle (θ_E), given by Young's relation[1] $\cos\theta_E = (\gamma_{sv} - \gamma_{sl})/\gamma_{lv}$. Here γ is the interfacial tension and the subscripts *s*, *l*, and *v* denote the solid, liquid, and vapor phase respectively. Altering the material chemistry of the solid surface changes the solid-liquid (γ_{sl}) and solid-vapor (γ_{sv}) interfacial tensions, thereby modifying the equilibrium contact angle (θ_E) for a given liquid on a solid surface. There are numerous reports of stimuli-responsive surface which alter their surface composition, and hence their wettability, in response to changes in temperature,[2] UV light,[3] pH,[4, 5] electrical voltage[6] and mechanical strain.[7] Switchable and tunable wettability for water[7, 8] (γ_{lv} = 72.1 mN/m) and also for low surface tension liquids[9] using mechanical strain as a stimulus has also been documented. While it is possible to control the contact angle of water droplets on flat surfaces from super-wetting ($\theta_E \sim 0°$, *e.g.* on clean silica) to partially non-wetting ($\theta_E \sim 125°$, *e.g.* fluorodecyl POSS),[10] the accessible range of equilibrium contact angles values (θ_E) for low surface tension liquids is rather limited. Indeed, there are no reports of natural or synthetic materials that display an equilibrium contact angle $\theta_E > 90°$ with low surface tension liquids such as methanol (γ_{lv} = 22.7 mN/m) and octane (γ_{lv} = 21.6 mN/m).

The observed contact angles for droplets of a low surface tension liquid can be increased significantly by texturing the contacting surface in order to trap numerous pockets of air underneath the liquid, thereby forming a composite (solid-liquid-air) interface. Previous work has shown that the presence of re-entrant surface texture (*i.e.* multivalued surface topography) is essential to support a composite interface with low surface tension liquids.[6, 10-15] There are numerous natural and synthetic surfaces that inherently incorporate re-entrant texture. Oleophobic surfaces can be realized by coating various re-entrant structures such as lotus leaves,[15] duck feathers,[9, 15] microfabricated surfaces,[6, 10, 16] and commercial fabrics[9, 17-19] to lower their surface energy (γ_{sv}). The inherent re-entrant texture of commercial fabrics enables them to serve as a class of model surfaces to study the effects of surface roughness, texture and surface energy on the wetting behavior of low surface tension liquids. There

have been numerous reports on hydrophobic[12, 19-21] and very recently oleophobic,[17, 18, 22] coated woven and non-woven fabrics that have exploited the underlying re-entrant texture of the fabric.

When a liquid droplet contacts a textured solid surface, it can either form a fully wetted (Wenzel)[23] interface with the liquid completely filling all the surface asperities, or a composite solid-liquid-vapor (Cassie-Baxter)[24] interface where numerous pockets of air are trapped underneath the contacting liquid. Classically, the apparent contact angle (θ^*) for a liquid droplet on a composite interface has been computed by using the Cassie-Baxter (CB) relation $\cos\theta^* = r_\phi\phi_s\cos\theta_E + \phi_s - 1$.[19, 25] Here r_ϕ is the roughness of the wetted area, ϕ_s is the area fraction of the liquid-air interface occluded by the solid texture, and θ_E is the equilibrium contact angle on a chemically identical smooth surface. Due to air entrapment in the composite state, it is possible to achieve high apparent contact angles ($\theta^* > 90°$) starting even with an inherently wetting surface (for which $\theta_E < 90°$), since as $r_\phi\phi_s \rightarrow 0$, $\theta^* \rightarrow 180°$. For a surface with a cylindrical texture characterized by radius R and inter-cylinder spacing $2D$, the CB relation can be rearranged into a more convenient form,[9, 15, 19] (Equation 1)

$$\cos\theta^* = -1 + \frac{1}{D^*}\left[(\pi - \theta_E)\cos\theta_E + \sin\theta_E\right] \qquad (1)$$

where $r_\phi = (\pi - \theta_E)/\sin\theta_E$, $\phi_s = R\sin\theta_E/(R+D)$, $D^* = (R+D)/R$. Note that the surface texture variables, r_ϕ and ϕ_s are functions of the equilibrium contact angle (θ_E) and are therefore dependent on the properties of the contacting liquid. In contrast, the spacing ratio (D^*) is a purely geometric parameter that helps to characterize the surface and relate the equilibrium contact angle (θ_E) as well as the topography of the texture with the apparent contact angle (θ^*).

The apparent contact angles obtained for a fully-wetted interface are predicted by the Wenzel relation[23] $\cos\theta^* = r\cos\theta_E$. Here the roughness r is the ratio of the *actual* solid-liquid interfacial area to the *projected* solid-liquid interfacial area. It should be noted that, in contrast to surfaces that can support a composite interface, surfaces that demonstrate large apparent contact angles in the Wenzel state require the smooth surface to be inherently non-wetting i.e. $\theta_E > 90°$. On the other hand, for an

inherently wetting surface i.e. $\theta_E < 90°$, the Wenzel state leads to significantly lower apparent contact angles. Further, it is clear from the Wenzel relation that as the roughness *r* becomes significantly greater than unity, the apparent contact angle $\theta^* \rightarrow 0°$ when $\theta_E < 90°$. In addition, previous work has also shown that as a consequence of the larger solid-liquid contact area in the fully wetted state, there is a higher chance of pinning of the solid-liquid-vapor triple phase contact line, which results in significant contact angle hysteresis (*i.e.* the difference between the apparent advancing and receding contact angles, $\Delta\theta = \theta^*_{adv} - \theta^*_{rec}$).[26]

The conditions for super-non-wettability, *i.e.* high apparent contact angles ($\theta^* > 150°$) and low contact angle hysteresis can be realized only in the case of a composite interface where the solid-liquid contact area is low. However for low surface tension liquids with $\theta_E < 90°$, the fully wetted or Wenzel state represents the thermodynamic equilibrium state, whereas the composite interface or the Cassie-Baxter state is at best metastable,[10, 11, 14, 15, 27-30] representing a local minimum in the overall free energy. Thus, for low surface tension liquids, the transition from a composite interface to a fully-wetted interface is irreversible and typically this transition leads to a loss of super-non-wettability. Therefore the ability to preserve this metastable composite interface is crucial for engineering non-wettable surfaces.

For a liquid droplet in a composite state, any pressure difference across the liquid-vapor interface (Laplace pressure or an applied external pressure) results in the sagging of the liquid-vapor interface. If this sagging becomes severe enough for the interface to touch the underlying level of solid texture, then the composite interface collapses and the liquid droplet rapidly transitions to a fully wetted state. The threshold pressure difference that triggers the transition is termed the breakthrough pressure ($P_{breakthrough}$).[15] To provide a quantitative measure of this breakthrough pressure, as well as the liquid non-wetting tendency of a composite interface, we have developed a design parameter framework which allows us to predict both the apparent contact angle (θ^*) and the robustness of the composite interface against external pressure perturbations which can lead to the wetting of a textured surface.[10, 15, 16] The

spacing ratio D^* (defined above) is the parameter that controls the degree of liquid wettability (the apparent contact angle θ^*, Equation 1). On the other hand, the robustness factor $A^* = P_{breakthrough} / P_{ref}$ compares the breakthrough pressure ($P_{breakthrough}$) required to force a given liquid-surface combination to undergo a wetting transition with the characteristic reference pressure, $P_{ref} = 2\gamma_{lv} / \ell_{cap}$.[15] Here ℓ_{cap} is the capillary length of the liquid ($\ell_{cap} = \sqrt{\gamma_{lv} / \rho g}$) and γ_{lv} is the liquid surface tension, ρ is the liquid density, and g is the acceleration due to gravity. A^* provides an *a priori* estimate of the robustness of a solid-liquid-vapor composite interface formed on a textured surface based on properties of the contacting liquid (ℓ_{cap}), surface texture parameters (R, D) and the interfacial properties of the triple phase contact line (θ_E). The reference pressure ($P_{ref} = 2\gamma_{lv} / \ell_{cap}$) is close to the minimum possible internal pressure in a millimetric-scale liquid droplet sitting on a highly non-wetting surface and therefore any surface-liquid combination for which $A^* \lesssim 1$ is unable to support a composite interface. For a cylindrical texture like a fabric surface, A^* takes the form:[9, 15]

$$A^* = \frac{P_{breakthrough}}{P_{ref}} = \frac{\ell_{cap}}{R(D^* - 1)}\left[\frac{(1 - \cos\theta_E)}{(D^* - 1 + 2\sin\theta_E)}\right] \quad (2)$$

At low values of the robustness factor ($A^* \approx 1$) the liquid-air interface sags significantly even under small pressure differentials and touches the next underlying level of surface texture. This sagging leads to an irreversible transition to the lower free energy Wenzel regime, which results in the loss of super-non-wettability. As a result, a high value of the robustness factor ($A^* > 1$) is an additional criterion beyond requiring a high value of the apparent contact angle (θ^*, Equation 1), when considering the design of super-non-wettable surfaces. For a given liquid (fixed ℓ_{cap}), the robustness factor (A^*) can be varied systematically, either by tuning the geometrical parameters[9] (R and D) describing the surface or by changing the equilibrium contact angle (θ_E) through modification of the surface chemical composition.

In a blend of two or more components, selective migration of the low surface energy component at the solid-air interface has been observed in many polymeric systems.[31] Bousquet and co-workers tracked this variation of the air-solid interfacial composition in a polymeric blend of polystyrene (PS) with polystyrene-*block*-polyacrylic acid (PS-b-PAA).[32, 33] In the as-cast state, the polymeric surface was rich in low surface energy polymer PS and the surface was enriched further after heating the sample in dry air at 95 °C for 3 to 5 days. In contrast, a similar heat treatment in a humid environment resulted in the enrichment of the more hydrophilic PAA towards the air-solid interface.

In the present work, the interfacial energy between the solid surface and the annealing medium is used to control the surface composition and thereby to modulate the surface energy of a novel polymeric coating deposited on top of a commercially available polyester fabric. A thermal annealing treatment in dry air or water is used to tune the solid surface energy (γ_{sv}) and the resulting apparent contact angles (θ^*). This surface tunability, combined with the inherent re-entrant texture of the underlying fabric, leads to a switchable liquid wetting surface even for low surface tension liquids like hexadecane (γ_{lv} = 27.5 mN/m) and dodecane (γ_{lv} = 25.3 mN/m).

Materials and Methods

Materials – We recently reported the synthesis of fluorodecyl POSS (polyhedral oligomeric silsesquioxane) molecules in which the silsesquioxane cages are surrounded by eight 1H,1H,2H,2H-heptadecafluorodecyl groups.[34] A smooth fluorodecyl POSS surface has one of the lowest solid surface energy values reported to date[15] ($\gamma_{sv} \approx$ 10 mN/m), due to the high density of perfluorinated carbon atoms present in the eight alkyl chains surrounding the silsesquioxane cages. To generate thin, uniform and flexible coatings of fluorodecyl POSS on the textures to be studied, polyethyl methacrylate (PEMA, Aldrich, molecular weight = 5.15 x 10^5 g/mol, $T_g \sim$ 65 °C) was used as the continuous polymeric matrix and Asahiklin (AK225, Asahi Glass Company) was used as the solvent for the polymer and fluorodecyl POSS.

Sample preparation and annealing – Silicon wafers were coated with a POSS (10 % by weight) - PEMA (90 % by weight) solution (total solids 10 mg/mL) by spin-coating at 900 rpm for 30 seconds. Commercially available polyester fabric (Anticon 100, commonly employed as a clean-room wipe) was used as the textured surface. The fabrics were dip-coated in a POSS (10%) – PEMA (90%) solution with a total solids concentration of 10 mg/mL. After immersion for 10 minutes, the dip-coated fabrics were removed and dried in a vacuum oven at 60°C for 30 minutes to ensure complete evaporation of the Asahiklin solvent. Annealing treatments were performed by heating the substrate in dry air or under DI water (resistivity > 18 MΩ-cm) at 90°C ($T > T_g$) and 1 atm pressure for three hours in an oven.

Surface characterization – Contact angle measurements were performed using a VCA2000 goniometer (AST Inc.). Advancing and receding contact angles were measured with ~5 μL droplets of various water-methanol mixtures and alkanes (purchased from Aldrich and used as received). AFM measurements were performed in the tapping mode using Veeco Metrology group, D3100 instrument. XPS characterization was carried out using a Kratos Axis Ultra x-ray photoelectron spectrometer manufactured by Kratos Analytical (Manchester, England). The monochromatized Al-K_α source was operated at 15 kV and 10 mA (150 W) and emissions were collected at take-off angles of 90° and 20° relative to the sample surface.

Results and Discussion

Contact angle measurements were performed on spin-coated silicon wafers in the original as-coated state (henceforth denoted by the notation - O) and also after consecutive annealing treatments of three hours at 90 °C, either in water followed by drying of the sample (denoted as - W) or in dry air (denoted as - A). The contact angles with water (γ_{lv} = 72.1 mN/m) displayed an oscillatory behavior for 2, 5, and 10 wt% POSS coating (Figure 1(a), (b), and (c) respectively) for four cycles of the two different annealing treatments. Higher contact angles were consistently observed for the original as-coated or air-annealed samples, in comparison to the corresponding water-annealed samples. Tapping mode AFM measurements showed that the rms roughness for all the samples considered range between

approximately 4 – 5 nm (Wenzel roughness, $r \approx 1.004$) and the roughness did not change appreciably after annealing. Therefore this variation in contact angles can be attributed to the variation of the surface chemical composition. The AFM phase images for air-annealed and water-annealed 10% POSS – 90% PEMA coatings on a silicon wafer are shown in Figure 1(d).

An identical sequence of annealing treatments resulted in a similar trend in the contact angle values for hexadecane (γ_{lv} = 27.5 mN/m) and other lower surface tension alkanes. The advancing contact angle (θ_{adv}) with hexadecane varied from 80 ± 2° on an air-annealed 10% POSS surface to 57 ± 4° on the corresponding surface annealed in water. The corresponding receding contact angles (θ_{rec}) were 56 ± 5° and 16 ± 2° respectively. Using the measured values of the advancing contact angle with water and alkanes, the surface energy of the air-annealed and water-annealed 10% POSS – 90% PEMA flat surface was estimated independently using both Zisman[35] (Figure 2) and the Owens-Wendt analysis.[36] Extrapolation of advancing contact angle data obtained for spin-coated flat silicon wafers with the homologous series of alkanes, yields critical surface tension values of $\gamma_c^{(air)} = 3 \pm 1.5$ mN/m for the air-annealed and $\gamma_c^{(water)} = 15.3 \pm 0.4$ mN/m for the water-annealed surface respectively. Although the data for the air-annealed state in Figure 2 show a clear linear variation with γ_{lv}, the critical surface tension determined by extrapolation in the Zisman analysis is unphysically low. This is because we expect the surface tension to be greater than $\gamma_{sv} \approx 6.7$ mN/m, the accepted minimum corresponding to a surface comprised of a monolayer of $-CF_3$ moieties.[35, 37] Although the actual numerical value of the critical surface tension (γ_c) is likely to be an artifact of the extrapolation procedure, the comparison of the two sets of advancing contact angle data obtained from the same experimental protocol is still instructive. The data illustrates that the surface energy of the 10% POSS – 90% PEMA surface in the water-annealed state (W) is considerably higher than the surface energy in the air-annealed state (A).

The polar and dispersive contributions to the solid-vapor interfacial energy (γ_{sv}) were determined by the Owens-Wendt analysis using water and octane as the probing liquids. For the 10% POSS – 90%

PEMA surface annealed in air, the polar component of the solid surface energy was $\gamma_{sv}^{p} = 0.3$ mN/m, with a dispersive component $\gamma_{sv}^{d} = 10.1$ mN/m, giving a total surface energy of $\gamma_{sv}^{(air)} = 10.4$ mN/m. Similarly, the polar component for the water-annealed surface was 1.3 mN/m and the dispersive component was 15.5 mN/m, leading to a total surface energy of $\gamma_{sv}^{(water)} = 16.8$ mN/m. The computed values of the estimated surface energy from Owens-Wendt analysis are more consistent with those expected for a fluorinated surface. These values again demonstrate that the surface energy is significantly higher after annealing in water (W) when compared to an identical surface annealed in air (A). For comparison, the estimated solid surface energy of a spin-coated PEMA surface is $\gamma_{sv} = 32$ mN/m ($\gamma_{sv}^{p} = 21$ mN/m and $\gamma_{sv}^{d} = 11$ mN/m). The low values of the solid surface energies estimated using the Owens-Wendt analysis also suggest a significant enrichment of the surface with the low surface energy fluorodecyl POSS species, for the air-annealed 10% POSS – 90% PEMA spin-coated surface.

This variation in the equilibrium contact angle on a flat surface, as highlighted in Figure 1, can be amplified by combining the aforementioned annealing treatment with a re-entrant textured surface such as that of a commercially available fabric. A polyester fabric (Anticon 100) was dip-coated in a 10% POSS – 90% PEMA solution to generate a re-entrant textured surface with a conformal and low surface energy coating. Figure 3(a) shows an SEM micrograph for a piece of the dip-coated polyester fabric, while Figure 3(b) shows an EDAX elemental mapping for fluorine in an identical region of the sample. Figure 3(b) indicates that the fluorodecyl POSS (the only species with fluorine) has conformally coated individual fibers of the fabric. The apparent contact angle (θ^{*}) measurements on the dip-coated fabric surface with water (γ_{lv} = 72.1 mN/m) are presented in Figure 4 (blue circles). It is clear that the observed apparent contact angles (θ^{*}) show an oscillatory behavior when the dip-coated fabric is successively annealed in water and dry air. The apparent advancing contact angle (θ_{adv}^{*}) with water (filled blue circles in Figure 4(a)) varies from $150 \pm 2°$ in the air-annealed state, to $140 \pm 3°$ in the water-

annealed state, whereas the corresponding apparent receding angle (θ^*_{rec}) (open blue circles in Figure 4(a)) ranges from $137 \pm 3°$ to $121 \pm 4°$. The robustness of this solid-liquid-air composite interface was computed using Equation 2 by assuming that the size of the fabric bundles as the dominant surface texture (i.e. assuming R = 100 μm, Figure 3(a)). For the smallest value of advancing contact angle on a smooth surface ($\theta_{adv} \sim 95°$ i.e. the advancing contact angle on the surface annealed in water), the robustness factor is found to be significantly greater than unity ($A^* \sim 2.4$). As a consequence, water forms a robust composite interface on both the air-annealed and water-annealed surfaces (Figures 4(b) and 4(c) respectively).

It is clear from Equation 2 that the robustness of the composite interface established by a liquid drop in contact with a re-entrant texture varies with the surface tension of the contacting liquid. Hexadecane droplets (γ_{lv} = 27.5 mN/m) form a robust metastable composite solid-liquid-air interface (with $\theta^*_{adv} = 135°$, $\theta^*_{rec} = 115°$ and $A^* \sim 1.4$) on both the original as-made (O) and air-annealed surfaces (A, Figure 4(b)). However when annealed in water, the advancing contact angle for hexadecane droplets on a flat surface reduces from $\theta^{(air)}_{adv} = 80 \pm 2°$ to $\theta^{(water)}_{adv} = 57 \pm 4°$. This reduction in the advancing contact angle on a flat surface (θ_{adv}) leads to a lowering of the robustness parameter (Equation 2; also see Figure S2) to approximately unity ($A^* \approx 0.9$), consequently the solid-liquid-air composite interface on the fabric transitions to the fully-wetted or Wenzel state ($\theta^*_{adv} \sim 0°$, $\theta^*_{rec} \sim 0°$, as shown in Figure 4(c)). As a result, switchable liquid wettability for hexadecane can be achieved between the two states, corresponding to a robust (but metastable) composite interface and a fully wetted interface, by using simple annealing treatments in air and water respectively (red squares in Figure 4(a)). Moreover, this switchability in the wetting behavior is repeatable, and the reversibility is demonstrated over five cycles of air and water annealing treatments (Figure 4(a)). The uncoated fabric and fabric coated with PEMA alone do not display any variation in the apparent contact angles with water and hexadecane after identical annealing treatments (Figure S1). Also, it is important to note that droplets of toluene or

acetone which are good solvents for PEMA wet the polyester fabric surface after it has been dip-coated either with 10% POSS – 90% PEMA or with pure PEMA. If such liquids are used for annealing treatment or contact angle measurements, the PEMA in the coating progressively dissolves in the solvent and the oleophobicity of the fabric surface is subsequently destroyed. Such effects may be mitigated in applications by using alternate elastomeric binders that can be chemically crosslinked following dip-coating.

The changes in the contact angles on flat (θ_E) and textured surfaces (θ^*) that result from annealing in air or water can be compactly represented in terms of a non-wetting diagram.[38-41] The variation in the cosine of the advancing apparent contact angle ($\cos\theta^*_{adv}$) on a dip-coated polyester fabric surface was plotted against the cosine of the advancing contact angle on a flat surface ($\cos\theta_{adv}$) as shown in Figure 5. The existence of a robust oleophobic textured surface is demonstrated by the data in the lower right quadrant (where $\theta_{adv} < 90°$ but $\theta^*_{adv} > 90°$, and henceforth denoted as Quadrant IV).

Figure 5 shows the observed advancing contact angle data for water-methanol mixtures (blue) and alkanes (red) on dip-coated polyester fabric. From the Zisman analysis (Figure 2) and Owens-Wendt analysis, it is clear that the air-annealed surface coating has a lower surface energy than the corresponding water-annealed 10% POSS – 90% PEMA coating. Therefore higher contact angles are observed for water-methanol mixtures (0 to 80% by volume methanol) on the air-annealed surface (A, blue filled circles in Quadrant III, where $\theta_{adv} > 90^\circ$ and $\theta^*_{adv} > 90^\circ$) compared to those on the water-annealed surface (W, blue open circles in Quadrants III and IV). Water-methanol mixtures up to 80% methanol by volume formed robust composite interfaces on fabric samples dip-coated in 10% POSS – 90% PEMA and subsequently annealed in either air (A) or water (W). On the contrary, lower surface tension liquids like hexadecane (γ_{lv} = 27.5 mN/m) and dodecane (γ_{lv} = 25.3 mN/m) switched from a robust metastable composite interface in the air-annealed state (A, red filled squares in Quadrant IV) to a fully wetted interface in the water-annealed state (W, red open squares in Quadrant I).

In order to explore the parameter space in Quadrant IV more effectively, the polyester fabric was dip-coated in pure PEMA solution ($\theta_{adv} = 78°$ with water) and contact angle measurements were performed on the textured PEMA surface. Water-methanol mixtures up to 40% methanol by volume formed a robust composite interface on the fabric dip-coated in PEMA alone (blue filled triangles in Quadrant IV). Mixtures with higher fractions of methanol wetted the PEMA-coated fabric spontaneously (blue filled triangles in Quadrant I). It is important to point out that once again the wetting behavior on PEMA coated fabric samples was independent of the annealing history.

The contact angle data on the three different coatings applied to the polyester fabric (*i.e.* (i) air annealed 10% POSS – 90% PEMA, (ii) water annealed 10% POSS – 90% PEMA, and (iii) pure PEMA), and with different polar (water-methanol mixtures) and non-polar liquids (various alkanes) were used to obtain the best fit value of the single geometric parameter D^* (see Equation 1) which characterizes the dip-coated polyester fabric. The black line shown in Figure 5 is the Cassie-Baxter equation for a surface composed of an aligned array of cylinders (Equation 1) with $D^* = 3.6 \pm 0.35$. This value of the spacing ratio (D^*) is obtained from the contact angle measurements alone and compares favorably with the value of the spacing ratio estimated by visual inspection of the SEM micrograph. Therefore, by measuring the variation in the apparent contact angles on a conformally coated textured surface, the fabric texture can be characterized in terms of the geometric spacing ratio D^*.

For the surfaces considered in Figure 5, the transition from a composite interface to a fully-wetted interface occurs at a critical contact angle on a flat surface $\theta_{crit} \sim 60°$. This sharp transition can be rationalized by considering the variation of the robustness factor A^*. The variation in the robustness factor A^* for hexadecane ($\gamma_{lv} = 27.5$ mN/m, $\ell_{cap} = 1.91$ mm) is plotted against the advancing contact angle on a flat surface (θ_{adv}) on the non-wetting diagram by using representative values of surface geometry parameters ($R = 100$ μm, $D^* = 3.6 \pm 0.35$). As the contact angle of the liquid on the flat surface decreases and $\cos\theta_E \rightarrow 1$, the robustness factor steadily decreases (Equation 2).[9, 15] When the

robustness factor (A^*) decreases towards values close to unity ($A^*_{crit} \approx 0.9$ in this case) the composite interface transitions to a fully-wetted interface. Note that the capillary length values for hexadecane (ℓ_{cap} = 1.91 mm) and 60% methanol – 40% water mixtures (ℓ_{cap} = 1.86 mm) are similar. Thereby, the critical robustness factor values for the water-methanol mixtures are similar to the values computed for hexadecane. The robustness parameter framework suggests that a metastable composite interface can be achieved only when $A^* > 1$, therefore the Cassie-Baxter prediction in Figure 5 is extended only up to a contact angle on a smooth surface at which $A^* \sim 1$.

From Equation 2 and Figure 5, it is clear that hexadecane droplets (γ_{lv} = 27.5 mN/m) will establish a robust metastable Cassie state on textures with $D^* \approx 3.6$ if the advancing contact angle on a flat surface is $\theta_{adv} > 60°$, but will transition to a fully-wetted Wenzel state if the contact angle is below $\theta_{adv} < 60°$ ($A^* \approx 1$). Variations in the apparent contact angle (θ^*) and design parameters (D^*, A^*) are outlined here for a particular fabric (Anticon 100) and a particular contacting liquid (hexadecane). However a similar framework can be developed for any liquid on any textured surface. By coating the texture with materials of various surface energy and performing contact angle measurements with a range of liquids, the textural parameters describing the surface can be fully characterized in terms of the dimensionless spacing ratio (D^*). Moreover having determined D^*, and knowing the equilibrium contact angle on a flat surface (θ_E) plus other physical properties of the liquid, the ability of a textured surface to support a composite interface with a given contacting liquid can be anticipated by computing the value of the robustness factor (A^*).

The observed changes in the macroscopic equilibrium contact angles (θ_E) (as highlighted in Figure 1) and the computed surface energy values can be related to molecular level rearrangements in the coating. The low surface energy component within the coating, i.e. fluorodecyl POSS ($\gamma_{sv} \approx 10$ mJ/m^2)[15] experiences a thermodynamic driving force to move towards the solid-air interface in order to minimize the solid-vapor interfacial free energy (γ_{sv}) of the POSS – PEMA coating. The

presence of solvent at the beginning of the drying step ensures high mobility of POSS, which facilitates its initial surface segregation. The fluorine to carbon (F/C) ratio for pure fluorodecyl POSS is 1.7 while it is 0 for pure PEMA. Based on these values, the F/C atomic ratio in the bulk of the 10% POSS – 90% PEMA sample can be readily computed to be 0.002. X-ray photoelectron spectroscopy (XPS) was used to probe the local composition of the surface (~ 10 nm probing depth).[42-44] XPS analysis was performed on spin-coated films of pure PEMA, pure fluorodecyl POSS and 10% POSS – 90% PEMA on silicon wafers and the results are summarized in Table 1. The various atomic ratios computed from the XPS survey spectra match reasonably with the computed values of the atomic ratios for pure PEMA and pure fluorodecyl POSS samples (Table 1).

The F/C ratios obtained from the survey spectra for air-annealed and water- annealed surfaces (Figure 6(a)) are 1.69 and 0.83 respectively. The greatly enhanced value of the F/C ratio at the surface (compared to the bulk) confirms the surface segregation of the low surface energy fluorodecyl POSS species. For the 10% POSS – 90% PEMA air-annealed samples, the atomic ratios (F/C, O/C and Si/C) are nearly equal to the corresponding ratios in the pure fluorodecyl POSS sample. This similarity in chemical composition and solid surface energy ($\gamma_{sv}^{(air)} = 10.4$ mJ/m^2) of the 10% POSS – 90% PEMA air-annealed samples to pure fluorodecyl POSS ($\gamma_{sv} \approx 10$ mJ/m^2)[15] indicates that the surface is mostly composed of fluorodecyl POSS. In contrast, significant lowering of the F/C ratio from 1.69 to 0.83, enhancement of the O/C ratio from 0.13 to 0.24, and increase in the solid surface energy from 10.4 to 16.8 mJ/m^2 indicate that the 10% POSS – 90% PEMA water-annealed surface has a higher PEMA content. Because the annealing treatment is carried out above the glass transition temperature ($T = 90$ °C $> T_g$), the PEMA chains at the surface have sufficient mobility to rearrange. This rearrangement of the PEMA chains can be tuned using the surface energy of the annealing media and is reversible over many cycles, as demonstrated through the variation of the equilibrium contact angles on a flat spin-coated surface (θ_E, Figure 1) and on polyester fabrics (θ^*, Figure 4). By lowering the take-off angle at which the photo-electrons are collected, even thinner sample interrogation volumes (sampling

depth < 10 nm) can be probed using XPS. When the samples were probed at a take-off angle of 20°, the F/C ratio was found to be higher than the F/C ratio obtained with 90° take-off angle (data presented in Table 1), for the corresponding air-annealed, as well as the water-annealed samples. This systematic variation in the F/C ratio indicates that the amount of fluorodecyl POSS is highest within the first few molecular layers from the surface, irrespective of the annealing condition. This observation suggests that the fluorodecyl POSS crystals as a whole are not migrating towards or away from the interface between the solid and the annealing medium (dry air or water), and PEMA rearrangement at the surface seems to be a more feasible explanation for our observations.

Further information about the chemical composition of the surface can be generated by examining high resolution carbon 1s spectra for samples annealed in air and water, as shown in Figures 6(b) and 6(c) respectively. Various peaks in the high resolution spectra were indexed by comparing the binding energy at the peak maximum with standard spectra available for PEMA and poly (vinylidene fluoride).[45] The spectrum for the air-annealed sample (Figure 6(b)) has a larger peak associated with the $–CF_2–$ moiety as compared to the peak associated with the $–CH_2–$ moiety, which once again indicates a larger surface presence of fluorodecyl POSS (which is the lone contributor to the $–CF_2–$ peak). On the other hand, for the case of the water-annealed sample (Figure 6(c)), the greater intensity of the $–CH_2–$ peak relative to the $–CF_2–$ peak confirms the presence of PEMA at the surface. Therefore, it can be concluded that the rearrangement of the PEMA chains at the surface is the main response to the annealing treatment. This subtle molecular response in the local chemical composition, when combined with a strongly re-entrant physical texture gives rise to non-wetting surfaces with switchable oleophobicity.

Conclusions

In the present work, we have demonstrated a novel methodology for obtaining surfaces with switchable liquid wettability. A commercially available polyester fabric was dip-coated with a mixture of a low glass transition temperature polymer PEMA ($T_g \approx 65$ °C) and an extremely low surface energy molecule

fluorodecyl POSS ($\gamma_{sv} \approx 10$ mJ/m^2). The combined effect of the re-entrant surface texture of the polyester fabric coupled with the relatively low T_g of PEMA, (which ensured sufficient mobility of the polymer chains at modest temperatures) led to a surface that exhibits switchable wettability with low surface tension liquids like hexadecane (γ_{lv} = 27.5 mN/m) and dodecane (γ_{lv} = 25.3 mN/m) in response to successive annealing treatments in water and dry air. Water-methanol mixtures and alkanes consistently exhibited higher contact angles on air-annealed 10% POSS – 90% PEMA coated surfaces than on the corresponding water-annealed surfaces. Advancing contact angle data on flat and textured surfaces were compactly displayed on a generalized non-wetting diagram and a critical robustness factor $A^*_{crit} \lesssim 1$ provided a quantitative criterion for the transition from a robust composite interface to a fully wetted interface.

Zisman and Owens-Wendt analyses indicated that the 10% POSS – 90% PEMA coating has a much lower surface energy ($\gamma_{sv}^{(air)} = 10.4$ mJ/m^2 and $\gamma_{sv}^{(water)} = 16.8$ mJ/m^2) than PEMA ($\gamma_{sv} = 32$ mJ/m^2) due to surface segregation of the low surface energy ($\gamma_{sv} \approx 10$ mJ/m^2) fluorodecyl POSS. XPS analysis confirmed surface segregation of fluorodecyl POSS through the high F/C ratios that were obtained at the surface compared to the bulk. After the volatile solvent evaporated, the bulk motion of the fluorodecyl POSS component was constrained but the PEMA chains could still surface-reorganize at temperatures above their glass transition temperature and this rearrangement was confirmed through XPS analysis. The rearrangement of the PEMA chains could be reversibly tuned by using the surface energy of the annealing media as the external stimulus. The measured contact angles and computed values of the surface energy correlated well with the subtle and reversible molecular rearrangement at the surface of the POSS – PEMA coating on the fibers.

ACKNOWLEDGMENT

This research was supported by the Army Research Office (ARO) through contract no. W911NF-07-D-0004 and the Air Force Research Lab (AFRL) under contract no. FA9300-06M-T015 and the Air Force Office of Scientific Research (AFOSR) under contract no. FA9550-07-1-0272 and LRIR-92PL0COR. We would like to thank Prof. Michael Rubner and the Institute of Soldier Nanotechnologies (ISN) at MIT for the use of various experimental facilities. Also, we would like to thank Elizabeth Shaw at the Center for Materials Science and Engineering (CMSE) at MIT for her help with the XPS and AFM and Mr. Jonathan DeRocher for his help during the preparation of this manuscript.

SUPPORTING INFORMATION

(i) Contact angle measurements on the polyester fabric without any coating as well as coated with polyethyl methacrylate (PEMA) only (Figure S1)

(ii) Schematic diagrams illustrating the role of the equilibrium contact angle on a flat surface (θ_E) on the sagging of the liquid-vapor interface and transition to the fully wetted state on a cylindrically textured surface (Figure S2)

(iii) XPS survey and carbon 1s high resolution spectra for pure PEMA and pure fluorodecyl POSS (Figure S3)

This information is available free of charge via the Internet at http://pubs.acs.org/.

TABLE CAPTIONS

Table 1. Computed atomic ratios and experimentally observed values from the XPS spectra for pure PEMA, pure fluorodecyl POSS and air-annealed (A) as well as water-annealed (W) 10% POSS – 90% PEMA spin-coated silicon wafer samples.

FIGURE CAPTIONS

Figure 1. Contact angle measurements on flat spin-coated surfaces (rms roughness < 5 nm) (a) Advancing (filled symbols) and receding (half-filled symbols) contact angles for water on 2 wt%, (b) 5 wt% and (c) 10 wt% fluorodecyl POSS-coated flat surfaces. The contact angles were measured in the original state (denoted as - O), after annealing in water at 90 °C for three hours followed by drying at room temperature (denoted as - W), and after annealing in air at 90 °C for three hours (denoted as - A). (d) AFM phase images of 10 wt% fluorodecyl POSS-coated flat surface after annealing in air (A) and in water (W).

Figure 2. Zisman analysis for 10% POSS – 90% PEMA spin coated film annealed in air (A, red filled squares) and annealed in water (W, red open squares). The contact angle data are measured with alkanes *i.e*. hexadecane (γ_{lv} = 27.5 mN/m), dodecane (γ_{lv} = 25.3 mN/m), decane (γ_{lv} = 23.8 mN/m), octane (γ_{lv} = 21.6 mN/m), and hexane (γ_{lv} = 18.5 mN/m) as contacting liquids and the critical surface tension for the solid surface is obtained by linear extrapolation of the contact angle data.

Figure 3. (a) An SEM micrograph of the polyester fabric Anticon 100 (b) EDAX fluorine elemental mapping of the identical area shown in Figure 3(a). The close correspondence between the two images confirms the conformal nature of the 10% POSS – 90% PEMA coating on the polyester fabric.

Figure 4. Switchable liquid wettability on a 10 wt% fluorodecyl POSS coated polyester fabric surface. (a) Apparent advancing (filled symbols) and receding (half-filled symbols) contact angle data with water (blue circles) and hexadecane (red squares) on 10 wt% fluorodecyl POSS-coated polyester fabric surface in the original as-made (O), water annealed (W), and air annealed (A) states. (b) Small droplets (V ≈ 50 μL) of water (γ_{lv} = 72.1 mN/m) and hexadecane (γ_{lv} = 27.5 mN/m) forming robust composite interfaces on the dip-coated fabric in the air annealed state (A). (c) Fully wetted hexadecane droplet

along with a water droplet forming a robust composite interface on the dip-coated fabric in the water annealed state (W).

Figure 5. Generalized non-wetting diagram for the dip-coated oleophobic polyester fabrics. Cosine of the apparent advancing contact angle ($\cos\theta^*_{adv}$) is plotted against the cosine of the advancing contact angle on a flat surface ($\cos\theta_{adv}$). Advancing contact angle data is shown for water-methanol mixtures (blue circles), and alkanes hexadecane (γ_{lv} = 27.5 mN/m) and dodecane (γ_{lv} = 25.3 mN/m) (red squares) on air-annealed (A, filled symbols) and water-annealed (W, open symbols) 10% POSS – 90% PEMA dip-coated surfaces. Advancing contact angles with water-methanol mixtures on PEMA-coated surface are also plotted (blue filled triangles). The black lines correspond to the Cassie-Baxter equation with D^* = 3.6 ± 0.35 (Equation 1). The blue lines are the robustness parameter (A^*) corresponding to R = 100 μm and D^* = 3.6 ± 0.35 plotted against the cosine of the advancing contact angle on a flat surface (θ_{adv}). The transition from a composite to a fully wetted interface takes place around $\theta_{crit} \approx 60°$.

Figure 6. XPS analysis of the 10 wt% fluorodecyl POSS – 90% PEMA dip-coated flat surface. (a) Survey spectra of the dip-coated surface annealed in water (W), showing major elemental peaks corresponding to F, O, C, and Si. (b) and (c) High resolution carbon 1s spectra for air-annealed (A) and water-annealed (W) dip-coated surfaces showing peaks corresponding to various carbon moieties present in the top layer (d ≤ 10 nm) of the POSS-PEMA coating.

REFERENCES

1. Young, T., *Philos. Trans. R. Soc. London* **1805,** 95, 65-87.
2. Sun, T.; Wang, G.; Feng, L.; Liu, B.; Ma, Y.; Jiang, L.; Zhu, D., *Angew. Chem. Int. Ed.* **2004,** 43, 357-360.
3. Feng, X.; Feng, L.; Jin, M.; Zhai, J.; Jiang, L.; Zhu, D., *J. Am. Chem. Soc.* **2004,** 126, 62-63.
4. Li, S.; Xie, H.; Zhang, S.; Wang, X., *Chem. Commun.* **2007**, 4857-4859.

5. Xia, F.; Ge, H.; Hou, Y.; Sun, T.; Chen, L.; Zhang, G.; Jiang, L., *Adv. Mater.* **2007,** 19, 2520-2524.

6. Ahuja, A.; Taylor, J. A.; Lifton, V.; Sidorenko, A. A.; Salamon, T. R.; Lobaton, E. J.; Kolodner, P.; Krupenkin, T. N., *Langmuir* **2008,** 24, 9-14.

7. Zhang, J.; Lu, X.; Huang, W.; Han, Y., *Macromol. Rapid Commun.* **2005,** 26, 477-480.

8. Feng, X.; Jiang, L., *Adv. Mater.* **2006,** 18, 3063-3078.

9. Choi, W.; Tuteja, A.; Chhatre, S.; Mabry, J. M.; Cohen, R. E.; McKinley, G. H., *Adv. Mater.* **2009,** 21, 2190-2195.

10. Tuteja, A.; Choi, W.; Ma, M.; Mabry, J. M.; Mazzella, S. A.; Rutledge, G. C.; McKinley, G. H.; Cohen, R. E., *Science* **2007,** 318, 1618-1622.

11. Cao, L.; Hu, H.; Gao, D., *Langmuir* **2007,** 23, 4310-4314.

12. Hoefnagels, H. F.; Wu, D.; deWith, G.; Ming, W., *Langmuir* **2007,** 23, 13158-13163.

13. Marmur, A., *Langmuir* **2008,** 24, 7573-7579.

14. Nosonovsky, M., *Langmuir* **2007,** 23, 3157-3161.

15. Tuteja, A.; Choi, W.; Mabry, J. M.; McKinley, G. H.; Cohen, R. E., *Proc. Natl. Acad. Sci. USA* **2008**, 18200-18205.

16. Tuteja, A.; Choi, W.; McKinley, G. H.; Cohen, R. E.; Rubner, M. F., *MRS Bull.* **2008,** 33, 752-758.

17. Brewer, S. A.; Willis, C. R., *Appl. Surf. Sci.* **2008,** 254, 6450-6454.

18. Leng, B.; Shao, Z.; de With, G.; Ming, W., *Langmuir* **2009,** 25, 2456-2460.

19. Michielsen, S.; Lee, H. J., *Langmuir* **2007,** 23, 6004-6010.

20. Ma, M.; Hill, R. M.; Rutledge, G. C., *J. Adhes. Sci. Technol.* **2008,** 22, 1799-1817.

21. Ma, M.; Mao, Y.; Gupta, M.; Gleason, K. K.; Rutledge, G. C., *Macromolecules* **2005,** 38, 9742-9748.

22. Han, D.; Steckl, A. J., *Langmuir* **2009,** In Press.

23. Wenzel, R. N., *Ind. Eng. Chem.* **1936,** 28, 988-994.

24. Cassie, A.; Baxter, S., *Trans. Faraday Soc.* **1944,** 40, 546-551.

25. Marmur, A., *Langmuir* **2003,** 19, 8343-8348.

26. Johnson, R.; Dettre, R., *Contact angle hysteresis. In Contact Angle, Wettability and Adhesion*. American Chemical Society: Wahington, D.C., 1964.

27. Herminghaus, S., *Europhys. Lett.* **2000,** 52, 165.

28. Cao, L.; Price, T. P.; Weiss, M.; Gao, D., *Langmuir* **2008,** 24, 1640-1643.

29. Kurogi, K.; Yan, H.; Tsujii, K., *Colloids Surf. Physicochem. Eng. Aspects* **2008,** 317, 592-597.

30. Jian-Lin, L.; Xi-Qiao, F.; Gangfeng, W.; Shou-Wen, Y., *J. Phys.: Condens. Matter* **2007,** 19, 356002.

31. Luzinov, I.; Minko, S.; Tsukruk, V. V., *Prog. Polym. Sci.* **2004,** 29, 635-698.

32. Bousquet, A.; Ibarboure, E.; Drummond, C.; Labrugere, C.; Papon, E.; Rodriguez-Hernandez, J., *Macromolecules* **2008,** 41, 1053-1056.

33. Bousquet, A.; Pannier, G.; Ibarboure, E.; Papon, E.; Rodriguez-Hernandez, J., *J. Adhes.* **2007,** 83, 335 - 349.

34. Mabry, J.; Vij, A.; Iacono, S.; Viers, B., *Angew. Chem. Int. Ed.* **2008,** 47, 4137-4140.

35. Zisman, W. A., *Relation of the equilibrium contact angle to liquid and solid construction*. American Chemical Society, Washington DC: 1964.

36. Owens, D. K.; Wendt, R. C., *J. Appl. Polym. Sci.* **1969,** 13, 1741-1747.

37. Nishino, T.; Meguro, M.; Nakamae, K.; Matsushita, M.; Ueda, Y., *Langmuir* **1999,** 15, 4321-4323.

38. Onda, T.; Shibuichi, S.; Satoh, N.; Tsujii, K., *Langmuir* **1996,** 12, 2125-2127.

39. Shibuichi, S.; Onda, T.; Satoh, N.; Tsujii, K., *J. Phys. Chem.* **1996,** 100, 19512-19517.

40. Quéré, D., *Rep. Prog. Phys.* **2005**, 2495.

41. Quéré, D., *Annu.Rev. Mater. Res.* **2008,** 38, 71-99.

42. Schmidt, D. L.; Coburn, C. E.; DeKoven, B. M.; Potter, G. E.; Meyers, G. F.; Fischer, D. A., *Nature* **1994,** 368, 39-41.

43. Ming, W.; van-de-Grampel, R. D.; Gildenpfennig, A.; Snijder, A.; Brongersma, H. H.; van-der-Linde, R.; de-With, G., *Polym. Mater. Sci. Eng.* **2003,** 88, 517.

44. Mao, Y.; Gleason, K. K., *Macromolecules* **2006,** 39, 3895-3900.

45. Beamson, G.; Briggs, D., *High resolution XPS of organic polymers: the Scientia ESCA300 database*. Wiley: New York, 1992.

TABLE OF CONTENT (TOC) IMAGE -

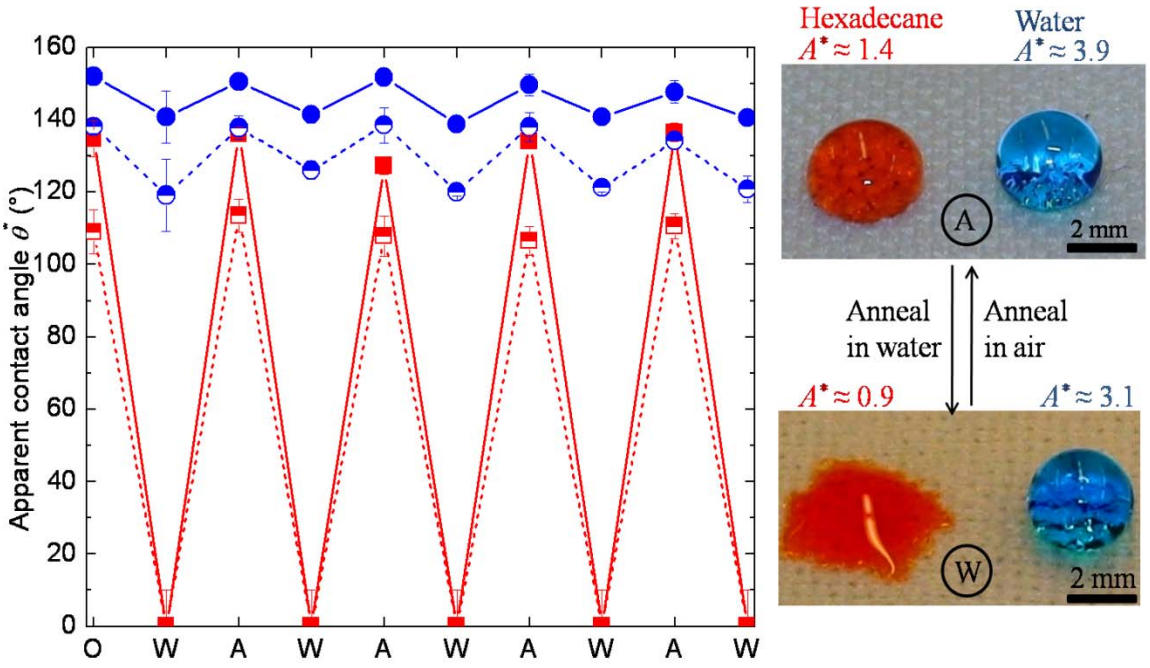

Switchable wettability for hexadecane ($\gamma_{lv} = 27.5$ mN/m) on a 10 wt% fluorodecyl POSS coated polyester fabric surface

Table 1. Computed atomic ratios and experimentally observed values from the XPS spectra for pure PEMA, pure fluorodecyl POSS and air-annealed (A) as well as water-annealed (W) 10% POSS – 90% PEMA spin-coated silicon wafer samples.

Sample description (take-off angle)		F / C	O / C	Si / C
PEMA	Computed	0	0.33	0
	Observed	0	0.27	0
POSS	Computed	1.7	0.15	0.1
	Observed	1.85	0.13	0.09
10% POSS – 90% PEMA	Computed	~0	~0.33	~0
	Air-annealed (90°)	1.69	0.13	0.07
	Water-annealed (90°)	0.83	0.24	0.05
	Air-annealed (20°)	1.91	0.14	0.08
	Water-annealed (20°)	1.41	0.20	0.07

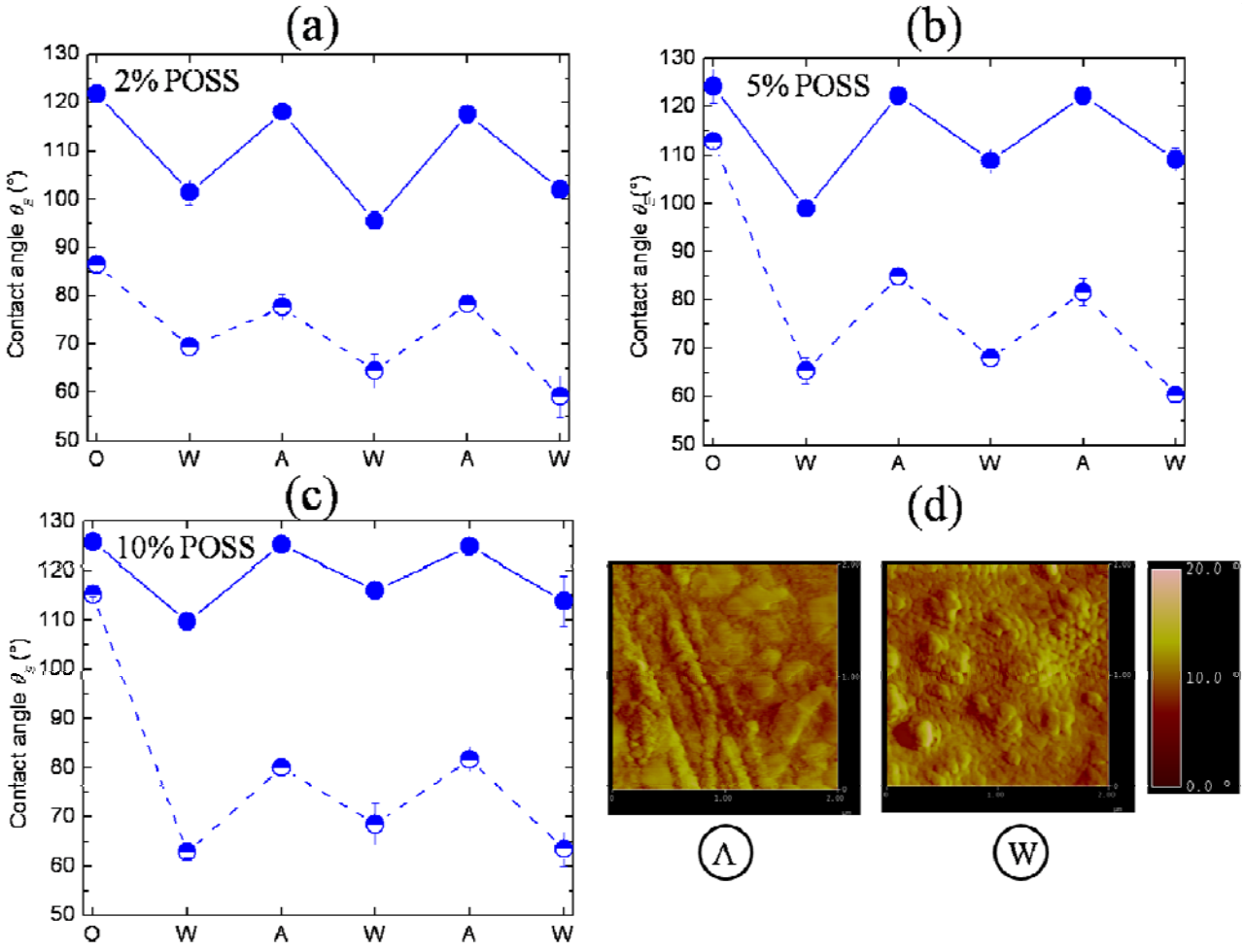

Figure 1. Contact angle measurements on flat spin-coated surfaces (rms roughness < 5 nm) (a) Advancing (filled symbols) and receding (half-filled symbols) contact angles for water on 2 wt%, (b) 5 wt% and (c) 10 wt% fluorodecyl POSS-coated flat surfaces. The contact angles were measured in the original state (denoted as - O), after annealing in water at 90 °C for three hours followed by drying at room temperature (denoted as - W), and after annealing in air at 90 °C for three hours (denoted as - A). (d) AFM phase images of 10 wt% fluorodecyl POSS-coated flat surface after annealing in air (A) and in water (W).

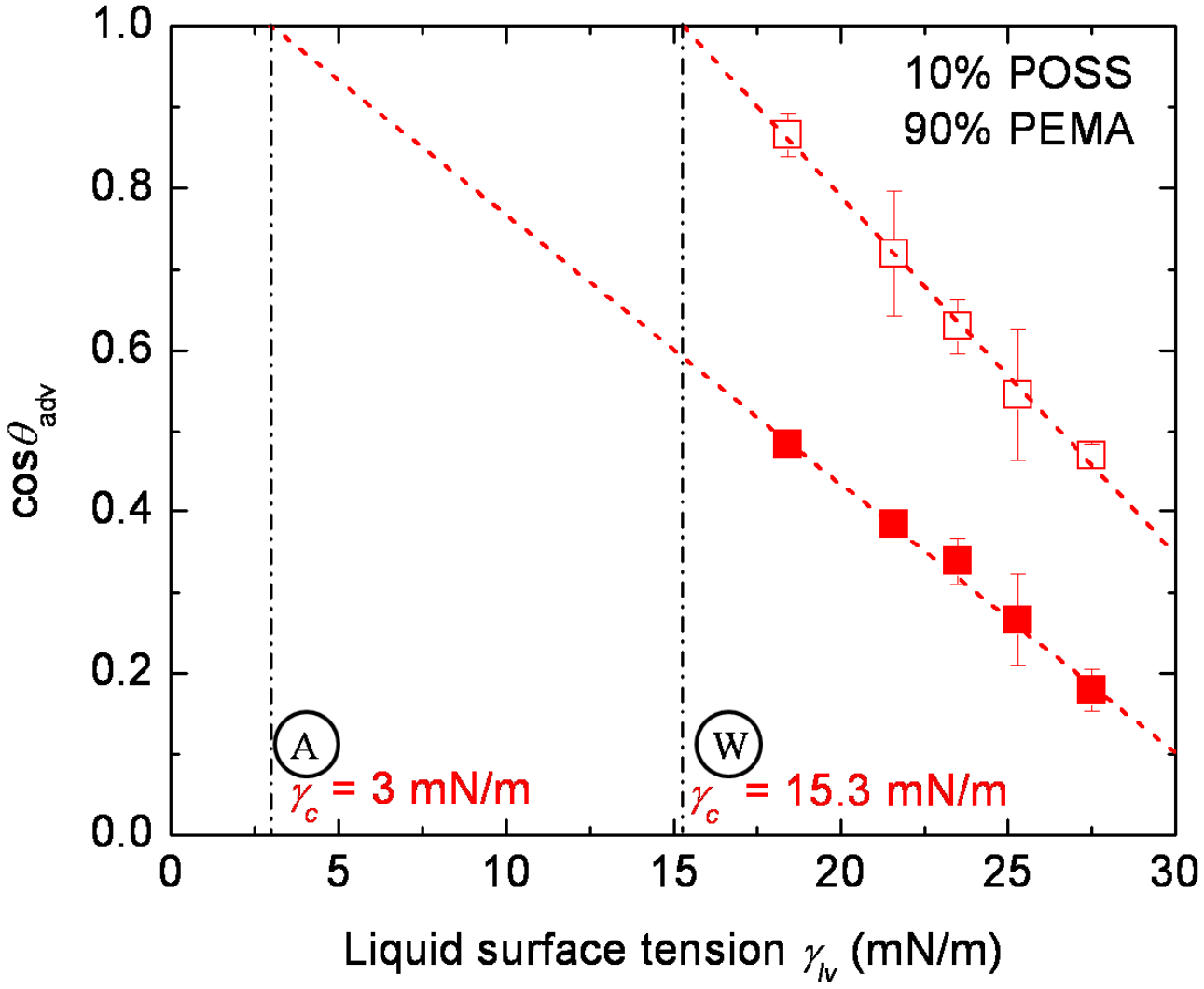

Figure 2. Zisman analysis for 10% POSS – 90% PEMA spin coated film annealed in air (A, red filled squares) and annealed in water (W, red open squares). The contact angle data are measured with alkanes *i.e.* hexadecane (γ_{lv} = 27.5 mN/m), dodecane (γ_{lv} = 25.3 mN/m), decane (γ_{lv} = 23.8 mN/m), octane (γ_{lv} = 21.6 mN/m), and hexane (γ_{lv} = 18.5 mN/m) as contacting liquids and the critical surface tension for the solid surface is obtained by linear extrapolation of the contact angle data.

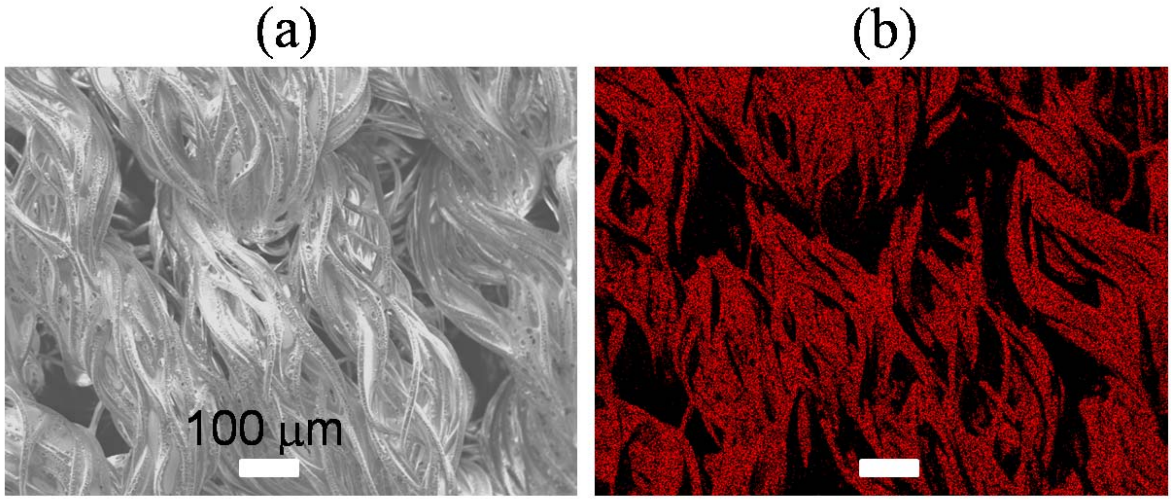

Figure 3. (a) An SEM micrograph of the polyester fabric Anticon 100 (b) EDAX fluorine elemental mapping of the identical area shown in Figure 3(a). The close correspondence between the two images confirms the conformal nature of the 10% POSS – 90% PEMA coating on the polyester fabric.

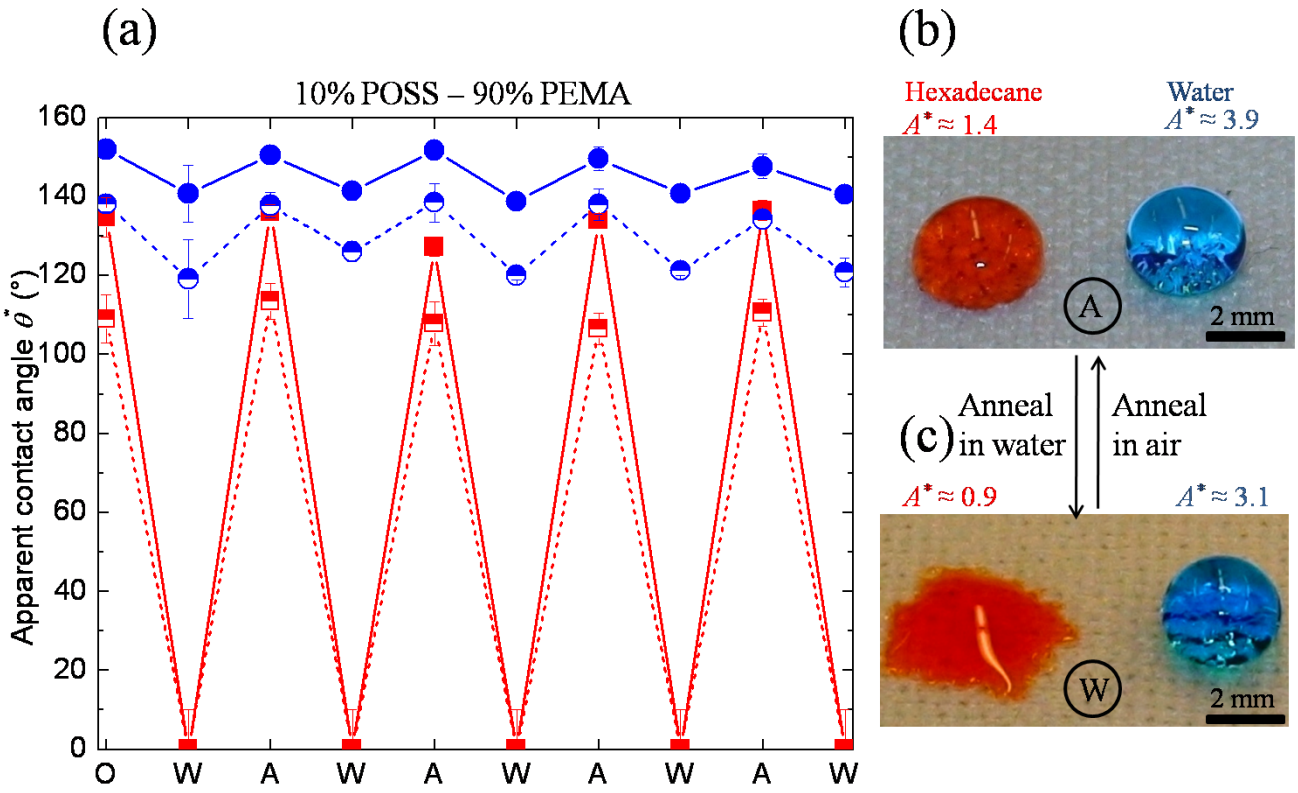

Figure 4. Switchable liquid wettability on a 10 wt% fluorodecyl POSS coated polyester fabric surface. (a) Apparent advancing (filled symbols) and receding (half-filled symbols) contact angle data with water (blue circles) and hexadecane (red squares) on 10 wt% fluorodecyl POSS-coated polyester fabric surface in the original as-made (O), water annealed (W), and air annealed (A) states. (b) Small droplets (V ≈ 50 μL) of water (γ_{lv} = 72.1 mN/m) and hexadecane (γ_{lv} = 27.5 mN/m) forming robust composite interfaces on the dip-coated fabric in the air annealed state (A). (c) Fully wetted hexadecane droplet along with a water droplet forming a robust composite interface on the dip-coated fabric in the water annealed state (W).

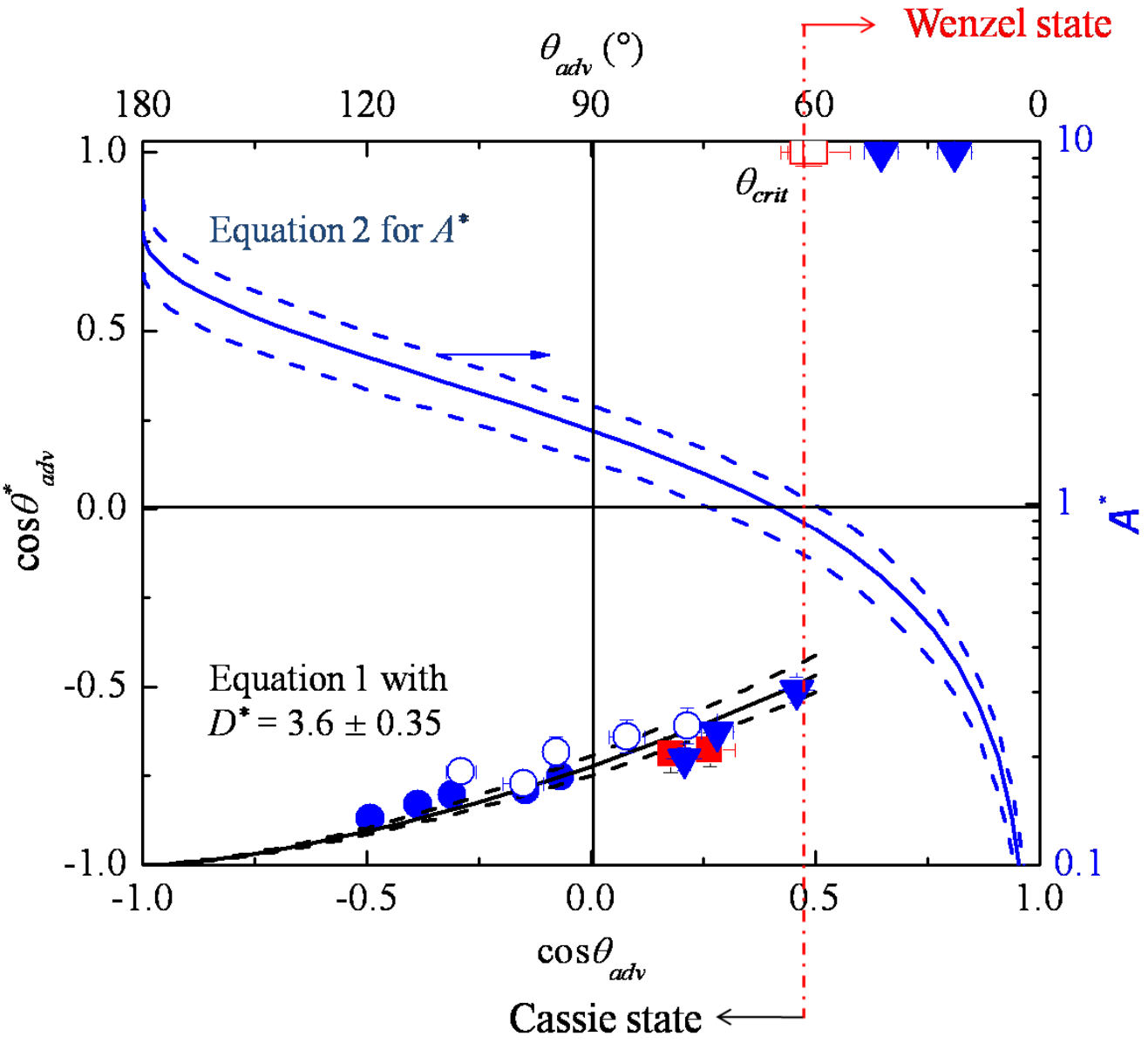

Figure 5. Generalized non-wetting diagram for the dip-coated oleophobic polyester fabrics. Cosine of the apparent advancing contact angle ($\cos\theta^*_{adv}$) is plotted against the cosine of the advancing contact angle on a flat surface ($\cos\theta_{adv}$). Advancing contact angle data is shown for water-methanol mixtures (blue circles), and alkanes hexadecane (γ_{lv} = 27.5 mN/m) and dodecane (γ_{lv} = 25.3 mN/m) (red squares) on air-annealed (A, filled symbols) and water-annealed (W, open symbols) 10% POSS – 90% PEMA dip-coated surfaces. Advancing contact angles with water-methanol mixtures on PEMA-coated surface are also plotted (blue filled triangles). The black lines correspond to the Cassie-Baxter equation with D^* = 3.6 ± 0.35 (Equation 1). The blue lines are the robustness parameter (A^*) corresponding to

$R = 100$ μm and $D^* = 3.6 \pm 0.35$ plotted against the cosine of the advancing contact angle on a flat surface (θ_{adv}). The transition from a composite to a fully wetted interface takes place around $\theta_{crit} \approx 60°$.

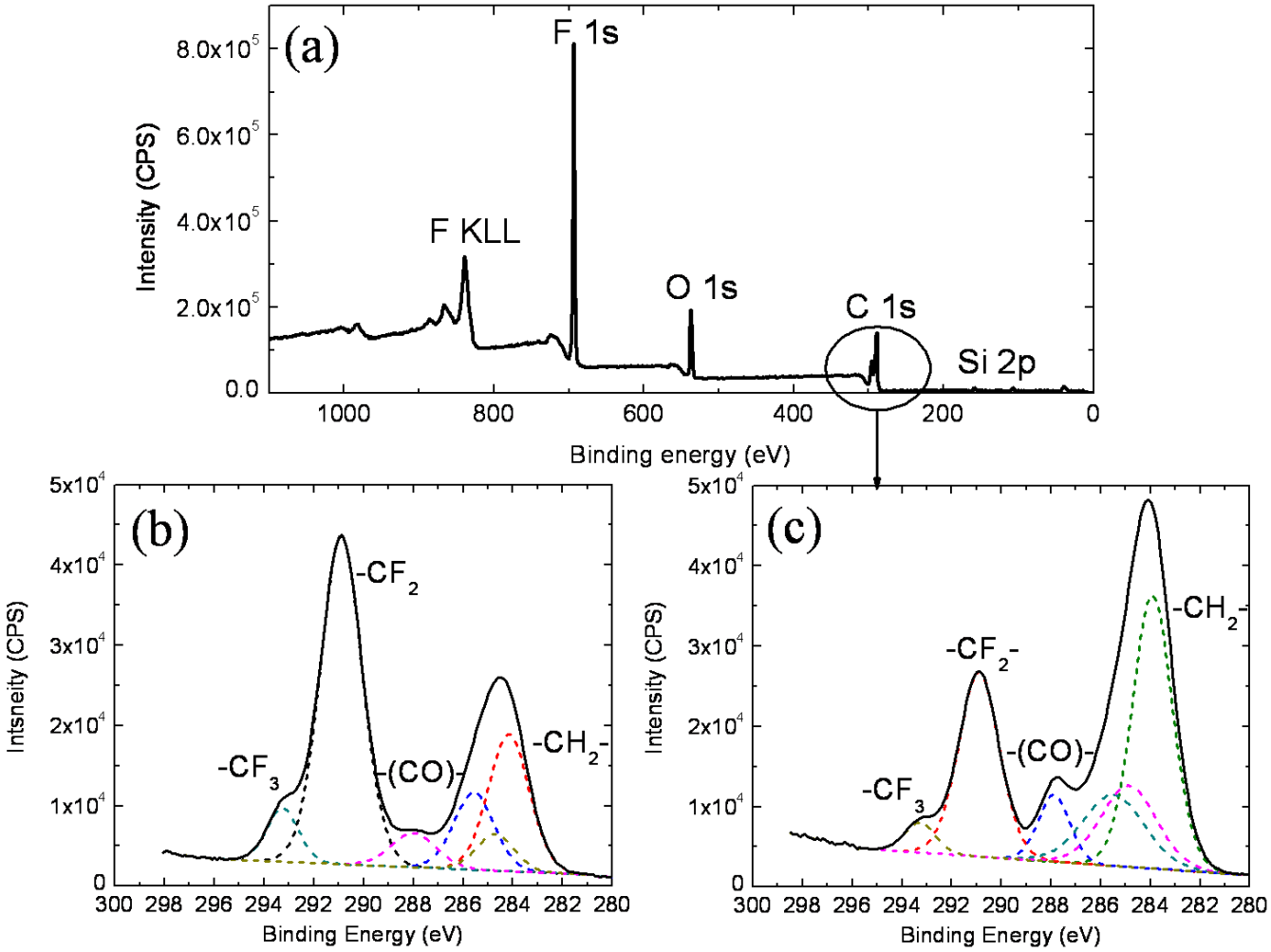

Figure 6. XPS analysis of the 10 wt% fluorodecyl POSS – 90% PEMA dip-coated flat surface. (a) Survey spectra of the dip-coated surface annealed in water (W), showing major elemental peaks corresponding to F, O, C, and Si. (b) and (c) High resolution carbon 1s spectra for air-annealed (A) and water-annealed (W) dip-coated surfaces showing peaks corresponding to various carbon moieties present in the top layer (d ≤ 10 nm) of the POSS-PEMA coating.

1. Control experiment (uncoated and PEMA-coated fabric)

Contact angle measurements were performed on the polyester fabric in the as-received, uncoated state and also after dip-coating in 10 mg/ml pure PEMA in Asahiklin (AK 225). No significant variation was observed in the apparent contact angles (θ^*) on these samples after a couple of annealing cycles in DI water at 90 °C and in dry air at 90 °C for 3 hours (results shown in Figure S1).

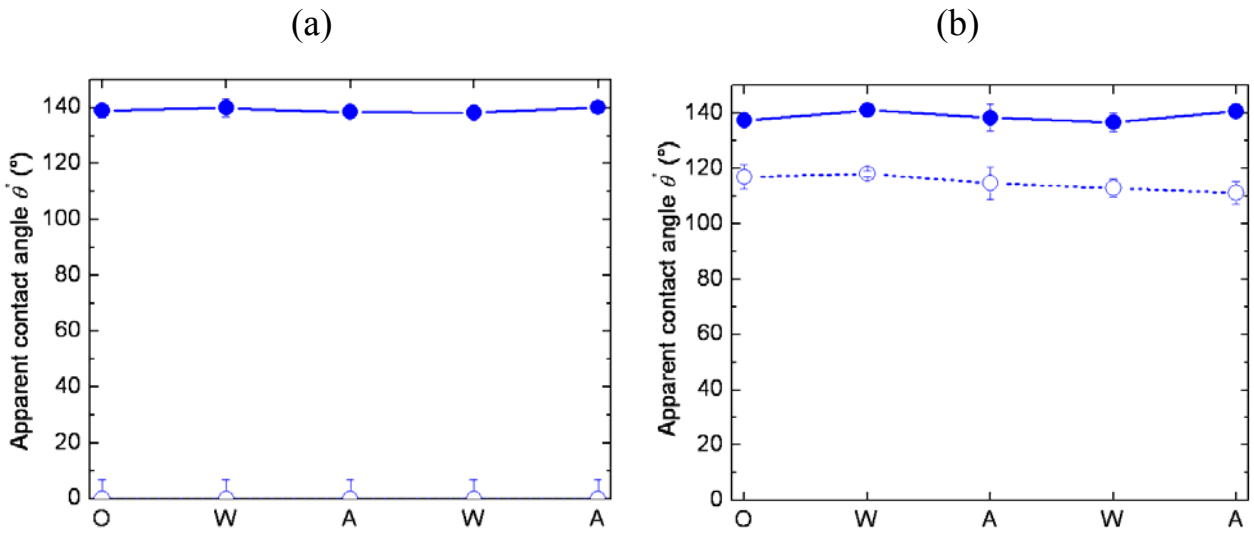

Figure S1. Variation in the apparent advancing (θ^*_{adv}) and receding (θ^*_{rec}) contact angles on polyester fabric (a) in the as-received uncoated state and (b) dip-coated with PEMA solution.

2. Schematic diagram of the sagging liquid-vapor interface

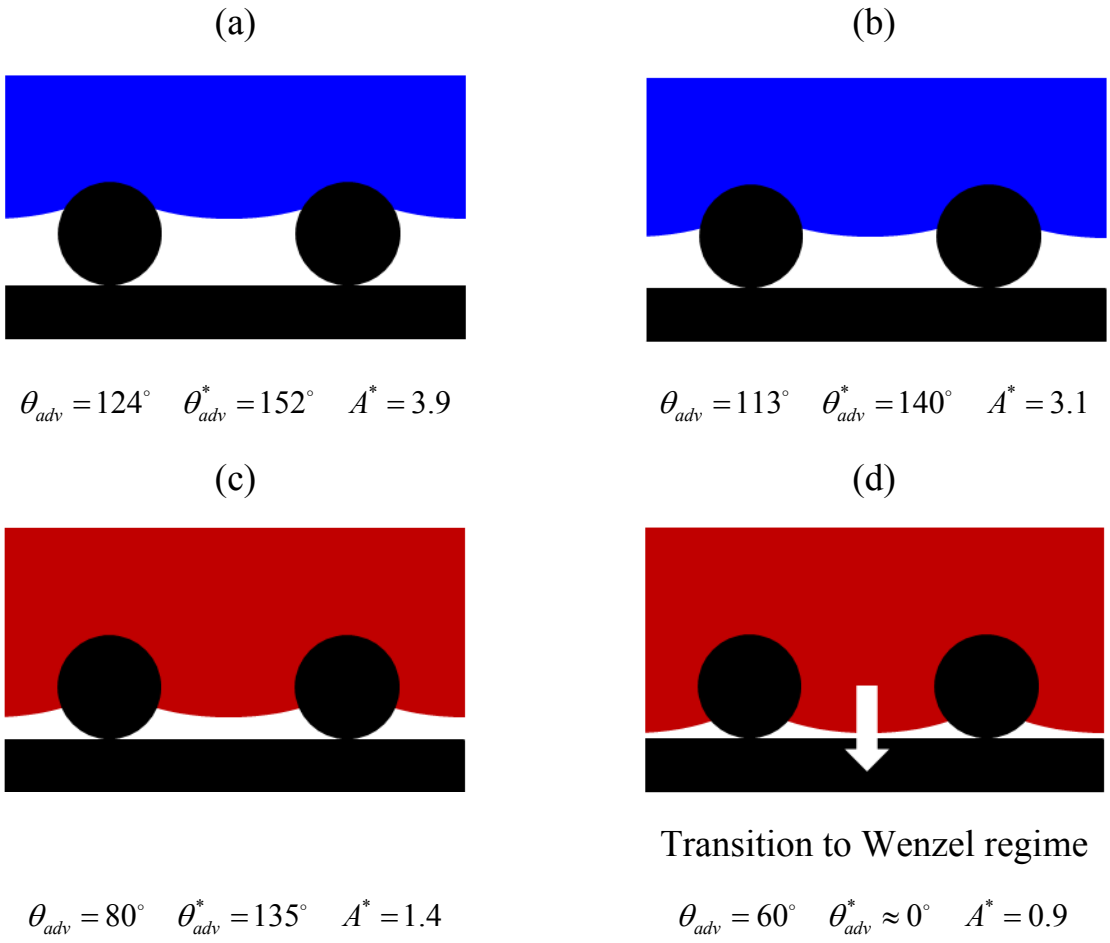

Figure S2. A schematic diagram illustrating the role of the equilibrium contact angle on a flat surface (θ_E) on the sagging of the liquid-vapor interface and transition to the fully wetted state on a cylindrically textured surface in the case of (a) water drop on an air-annealed (A) 10% POSS – 90% PEMA coated surface, (b) water drop on a water-annealed (W) 10% POSS – 90% PEMA coated surface, (c) hexadecane drop on an air-annealed 10% POSS – 90% PEMA coated surface, and (d) hexadecane drop on a water-annealed 10% POSS – 90% PEMA coated surface, which transitions into the fully wetted regime.

3. XPS data – for pure PEMA and POSS

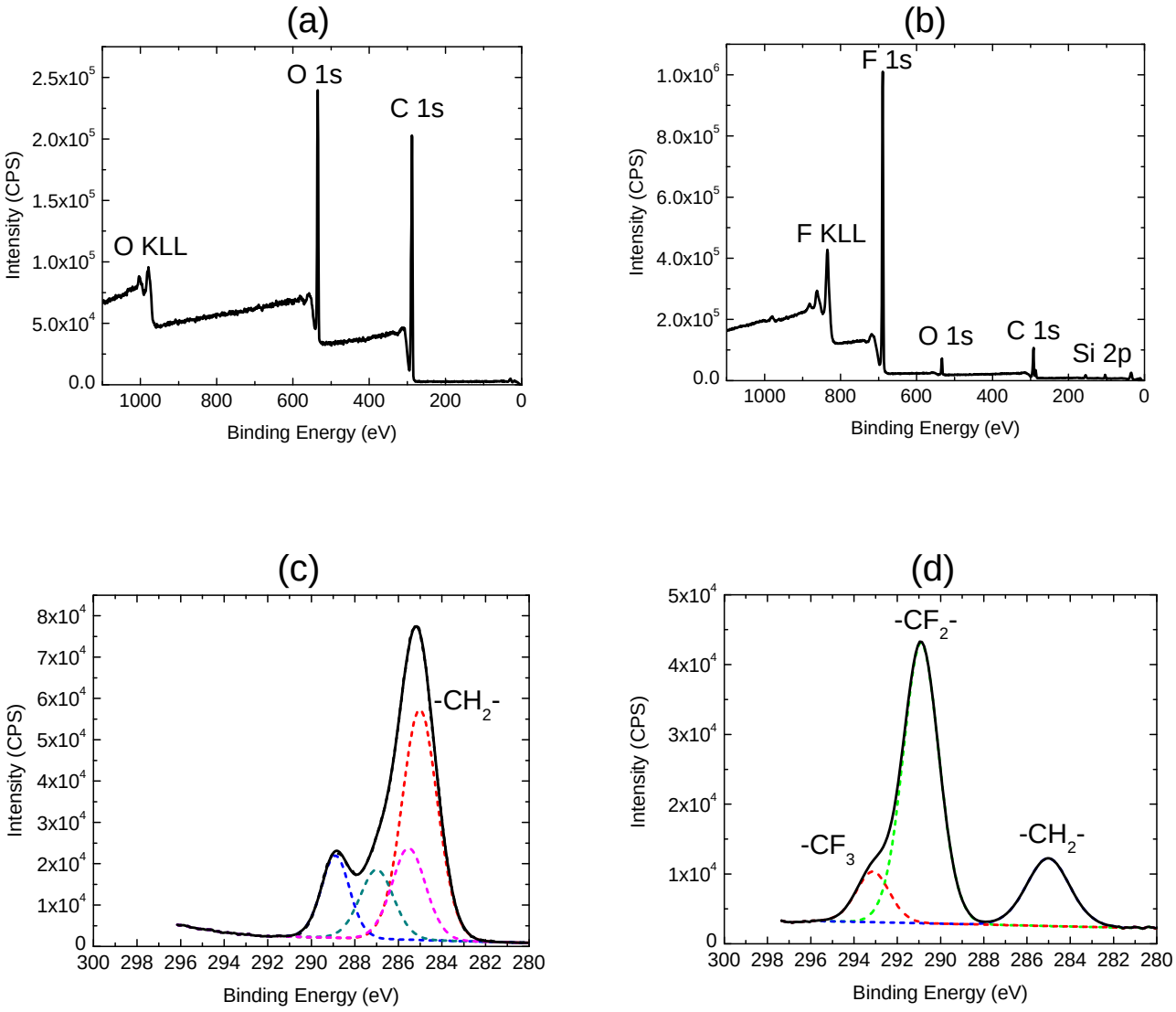

Figure S3. Survey spectra for (a) PEMA and (b) fluorodecyl POSS showing the characteristic peaks for carbon, oxygen, silicon, and fluorine and high resolution carbon 1s spectra for (c) PEMA and (d) fluorodecyl POSS are shown.